arXiv:1304.1734v1 [cond-mat.mes-hall] 5 Apr 2013

Bilayer graphene heterostructure with hBN: Interplay between misalignment, interlayer asymmetry, and trigonal warping

M. Mucha-Kruczyński,*,† J. R. Wallbank,† and V. I. Fal'ko†

Department of Physics, Lancaster University, Lancaster, LA1 4YB, United Kingdom, and
Department of Physics, University of Bath, Claverton Down, Bath BA2 7AY, United Kingdom

E-mail: m.mucha-kruczynski@bath.ac.uk

Abstract

We show that a slightly incommensurate hexagonal substrate (e.g., hexagonal boron nitride) applied to one side of bilayer graphene (BLG) with Bernal stacking inflicts inversion symmetry breaking and opens gaps in the spectrum of minibands created by the periodic moiré pattern. This contrasts the behaviour of moiré minibands in monolayer graphene, where well-resolved minibands are connected by Dirac points.

The heterostructures of graphene with other hexagonal layered crystals or crystals with hexagonal symmetry facets feature moiré patterns which are the result of incommensurability of the periods of the two two-dimensional lattices, or their misalignment. Since the period of the moiré pattern is longer for a pair of crystals with a closer size of lattice constants and better aligned principal crystallographic axes, the long period moiré superlattices are characteristic for graphene/hexagonal boron nitride (hBN) heterostructures with a small misalignment angle θ between the two honeycomb lattices. Such heterostructures have recently been created by transferring graphene onto hBN.[1–4] The influence of hexagonal moiré patterns on Dirac electrons in monolayer graphene (MLG) has been studied in detail,[1–8] both using specific microscopic models and phenomenologically. Three possible types of moiré miniband structures on the conduction/valence band sides of graphene's spectrum have emerged from the theories:[2–8] sometimes, spectra without a distinct separation between the lowest and other minibands; quite exceptionally, the first miniband separated from the next band by a triplet of secondary Dirac points (sDPs) in each of the graphene valleys K and K'; more generically, a single sDP at the edge of the first miniband in each valley. Also, the signatures of the miniband formation have been observed experimentally in the tunneling density of states[2] and magnetotransport characteristics[3,4] in MLG/hBN heterostructures.

---

*To whom correspondence should be addressed

†Department of Physics, Lancaster University, Lancaster, LA1 4YB, United Kingdom

‡Department of Physics, University of Bath, Claverton Down, Bath BA2 7AY, United Kingdom

In this Letter, we analyze the characteristic moiré miniband features in heterostructures of bilayer graphene (BLG) with highly oriented and almost commensurate, hexagonal crystals, such as hBN, recently created and investigated using magneto-transport measurements by Dean et al.[9] We find that, in contrast to monolayers, the electronic spectrum of BLG on hBN is most likely to exhibit global gaps between the first moiré miniband and the rest of the spectrum (on either valence or conduction band side, but sometimes in both bands), or have the bands strongly overlapping with each other, but almost never has Dirac points at the miniband edge. This behaviour is prescribed by the substrate creating a moiré perturbation only for one layer of BLG, thus breaking the inversion symmetry of the moiré superlattice. This point becomes apparent from the parametric space diagrams in Fig. 1, where the regions of the parameter space with gapped spectra are painted in red with an overlapping (non-resolved) bands - left transparent. Differences between the two diagrams corresponding to different misalignment angles θ arise from the interplay between the orientation of the supercell Brillouin zone (sBZ) and interlayer hopping in BLG.

The above conclusions are derived using a phenomenological approach[8] which involves the description of the long-range moiré superlattice using a Dirac-type model for graphene electrons, where we include the dominant harmonics in the moiré perturbation and perform an exhaustive

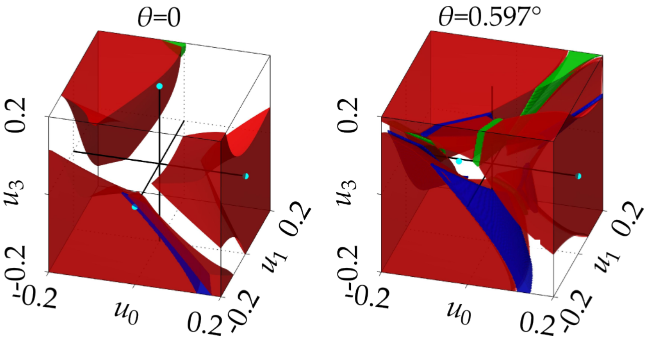

Figure 1: Parameter space (u_0, u_1, u_3) used to classify characteristic behaviour of moire miniband in highly oriented BLG on almost commensurate substrate: in red, we paint regions where BLG spectrum has a gap separating the first miniband in the valence band from the rest of the spectrum, regions with overlapping (unresolved) bands are transparent and blue/green mark the degenerate conditions for the appearance of isolated secondary Dirac points at the first miniband edge, like in monolayer graphene.[2,6–8] A similar parametric plot describing the minibands on the conduction band side can be obtained by inversion in the u_0-u_3 plane.

numerical analysis in order to characterise the miniband behaviour over a broad range of the parameter space. For BLG placed on top of a substrate with hexagonal symmetry and the lattice constant $a_S = (1+\delta)a$ larger by δ than that of graphene, (a=2.46Å, and for the case of hBN, $\delta = 1.8\%$[1]), the lattice mismatch, together with a possible misalignment of the two lattices given by the angle θ, lead to a periodic structure which can be described using a set of reciprocal lattice vectors,

$$b_n = \hat{R}_{n\pi/3}\left[1-(1+\delta)^{-1}\hat{R}_\theta\right](0, \frac{4\pi}{\sqrt{3}a}), \quad n = 0, 1, \ldots, 6,$$

where $\hat{R}_\varphi$ stands for anticlockwise rotation by angle φ and $b = |b_n| \approx \frac{4\pi}{\sqrt{3}a}\sqrt{\delta^2+\theta^2}$.[4] Note that this set both rotates by $\phi(\theta)$ and changes its size as a function of θ, Fig. 2. The electrons in BLG/hBN

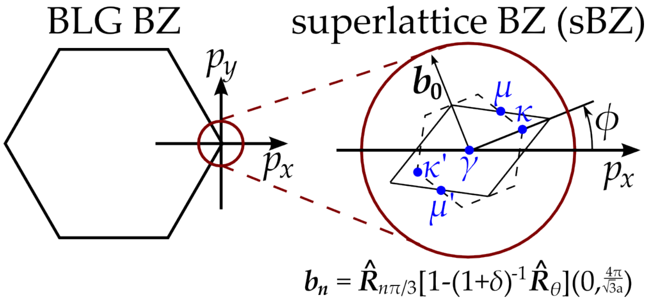
BLG BZ
superlattice BZ (sBZ)
p_y
p_x
$\boldsymbol{b}_0$
μ
κ
ϕ
κ'
γ
μ'
p_x
$\boldsymbol{b}_n = \hat{\boldsymbol{R}}_{n\pi/3}[1\text{-}(1\text{+}\delta)^{-1}\hat{\boldsymbol{R}}_\theta](0,\frac{4\pi}{\sqrt{3}a})$

Figure 2: Hexagonal Brillouin zone (BZ) of BLG with the valley coordinate system p_x, p_y and the electronic bands in the vicinity of the K valley, together with the zoom in on the supercell Brillouin zone (sBZ) where we mark its own symmetry points κ and μ.

heterostructure are described by the Hamiltonian

$$\hat{H}=\begin{pmatrix} v_3(\sigma\cdot p)^T & v\sigma\cdot p \\ v\sigma\cdot p & \gamma_1\sigma_x\tau_z \end{pmatrix}+$$

$$\frac{1}{2}vb\left[\begin{pmatrix} g_+(r)(1+\sigma_z\tau_z) & 0 \\ 0 & g_-(r)(1-\sigma_z\tau_z) \end{pmatrix}-\begin{pmatrix} 0 & g^*(r)(\tau_z\sigma_x+i\sigma_y) \\ g(r)(\tau_z\sigma_x-i\sigma_y) & 0 \end{pmatrix}\right], \tag{1}$$

$$g_\pm(r)=u_0\sum_n e^{ib_n\cdot r}\pm iu_3\sum_n(-1)^n e^{ib_n\cdot r},\quad g(r)=(u_2+iu_1\tau_z)\sum_n(-1)^n e^{ib_n\cdot r}(\hat{b}_n^x+i\hat{b}_n^y\tau_z),\quad b_n=b(\hat{b}_n^x,\hat{b}_n^y),$$

written in the basis[10] of the Bloch states on sublattices $\{\phi(A_1),\phi(B_2),\phi(A_2),\phi(B_1)\}$ in the K valley and $\{\phi(B_2),-\phi(A_1),\phi(B_1),-\phi(A_2)\}$ in K', where indices 1/2 mark the bottom/top layers and the substrate directly acts on the electrons in the bottom layer. We also use $\hbar=1$ and employ two sets of Pauli matrices σ_i, $\sigma=(\sigma_x,\sigma_y)$, and τ_i, acting in the sublattice and valley space, respectively.

The first matrix on the left-hand side of Eq. (**??**) follows from the tight-binding description of BLG,[11] with $v=10^6$m/s resulting from the interlayer hopping in graphene. The 'vertical' interlayer hopping between the closest neighbours is taken into account by parameter $\gamma_1=0.38$eV,[12] and the skew next-neighbour interlayer hopping, γ_3, is taken into account by the 'trigonal warping term',[11–13] with $v_3\approx 0.1v$. This results in the four-band BLG model, with two bands degenerate at the points K and K', and two bands split away by $\pm\gamma_1$.

The next two terms on the right-hand side of Eq. (**??**), scaled using energy scale vb and parametrised using dimensionless $u_{0,1,2,3}$,[8] describe the effect of the substrate on BLG through its coupling with carbon orbitals in the closest, bottom layer. The parameter u_0 characterizes the magnitude of the perturbing potential, u_3 captures the local asymmetry between the A_1 and B_1 sublattices, whereas u_1 and u_2 introduce modulation of the in-plane hops for the electrons travelling within the bottom layer. As opposed to the monolayer case,[8] the u_2 term cannot be completely gauged away but its effect on the band structure is generated only via the interplay with the trigonal warping term, and hence is small, so that we neglect it in further discussions. Note that, since we scale all energies using the scale vb set by the periodicity of the moiré pattern, the size of dimensionless parameters u_i in Eq. (**??**) would be larger for smaller angle θ for the same pair of BLG and substrate crystal.

For the sake of a systematic comparison with the low-energy 'two-band' model of free-standing BLG,[11] applicable at the energy scale $\varepsilon \ll \gamma_1$, we use a Schrieffer-Wolff transformation[14] and project the four-band Hamiltonian onto the low-energy bands, reducing it to an effective two-band Hamiltonian,

$$\begin{aligned}&\hat{H}_{\text{eff}} \approx -\frac{v^2}{\gamma_1}\left[(p_x^2-p_y^2)\sigma_x+2p_xp_y\sigma_y\right]\tau_z+v_3(\sigma\cdot p)^T+\\&\frac{vb}{2}g_+(r)(1+\sigma_z\tau_z)+\frac{v^3b}{2\gamma_1^2}(p_x-i\sigma_zp_y)g_-(r)(p_x+i\sigma_zp_y)(1-\sigma_z\tau_z)+\\&\frac{v^2b}{2\gamma_1}[(p_x+ip_y\tau_z)g(r)(\sigma_x-i\sigma_y\tau_z)+g^*(r)(p_x-ip_y\tau_z)(\sigma_x+i\sigma_y\tau_z)].\end{aligned} \tag{2}$$

The applicability of the simplified Hamiltonian to the description of, at least, the first moiré miniband in the BLG spectrum requires that $\gamma_1 \gtrsim 2vb$. For a perfectly aligned BLG/hBN heterosystem, we estimate that $\frac{\gamma_1}{vb} \approx \frac{\sqrt{3}}{4\pi}\frac{a\gamma_1}{v}\frac{1}{\sqrt{\delta^2+\theta^2}} = 1.08$, which suggests that a quantitative description of moiré minibands in BLG/hBN requires the use of the four-band Hamiltonian, Eq. (**??**).

From this point, the analysis of moiré minibands in BLG consists in a systematic zone folding and numerical diagonalization of the four-band Hamiltonian $\hat{H}$. Due to the time-inversion of the

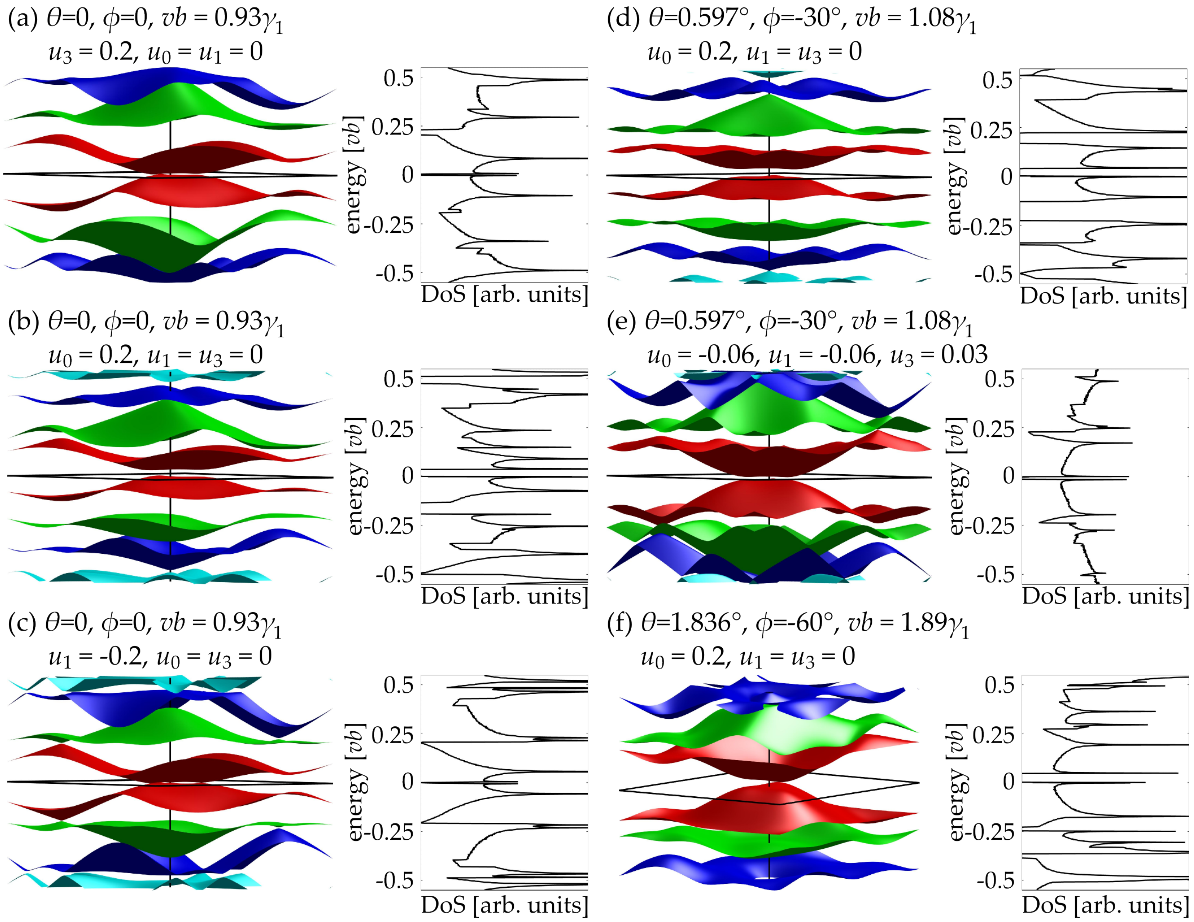

(a) θ=0, ϕ=0, vb = 0.93γ_1 u_3 = 0.2, u_0 = u_1 = 0

(b) θ=0, ϕ=0, vb = 0.93γ_1 u_0 = 0.2, u_1 = u_3 = 0

(c) θ=0, ϕ=0, vb = 0.93γ_1 u_1 = -0.2, u_0 = u_3 = 0

(d) θ=0.597°, ϕ=-30°, vb = 1.08γ_1 u_0 = 0.2, u_1 = u_3 = 0

(e) θ=0.597°, ϕ=-30°, vb = 1.08γ_1 u_0 = -0.06, u_1 = -0.06, u_3 = 0.03

(f) θ=1.836°, ϕ=-60°, vb = 1.89γ_1 u_0 = 0.2, u_1 = u_3 = 0

Figure 3: (a-e) Moiré miniband spectra (drawn within the rhomboidal sBZ) and density of states (DoS) for $\theta = 0$ and $\theta = 0.597°$ and several points in the (u_0, u_1, u_3) parameter space as marked in Fig. 1. Also, an example of the spectrum for large misalignment angle is shown in (f). In cases (b,d,f), a sizeable gap is visible between the conduction and valence gap of BLG, opened due to the interlayer asymmetry generated by the moiré perturbation of the substrate applied only to one layer.

problem,[15]

$$\hat{H}(p) = \sigma_y \tau_y \left[\hat{H}(-p)\right]^T \sigma_y \tau_y,$$

electronic spectra in the two valleys are related, $\varepsilon_{K+p} = \varepsilon_{K'-p}$, and in the following, we only discuss electronic spectra in valley K. Moreover, using the commutation properties of the Pauli matrices,

(a) θ=0, ϕ=0, vb = 0.93γ_1
u_0 = 0.2, u_1 = u_3 = 0, δ = -0.041eV

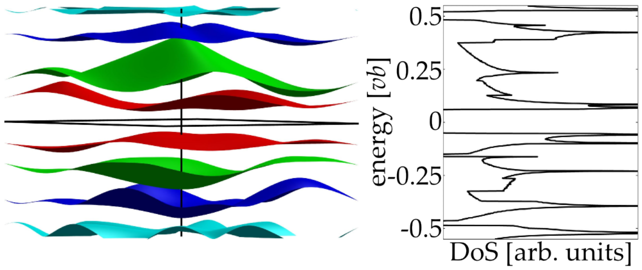

(b) θ=0.597°, ϕ=-30°, vb = 1.08γ_1
u_0 = -0.06, u_1 = -0.06, u_3 = 0.03, δ = -0.056eV

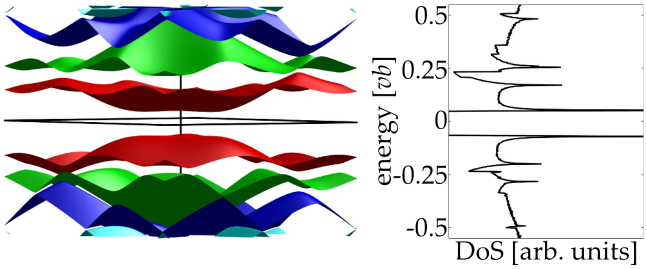

Figure 4: Examples of the miniband spectra and DoS for structures doped up to four holes per moire supercell using a single side gate. By inspection, one can find that constant in space interlayer asymmetry, leading to a sizeable gap between valence and conduction bands of BLG, does not affect the occurrence of a gap or the overlap between the first and next minibands in the superlattice spectrum.

one finds that for the band structure within the same valley,

$$\varepsilon_{K+p}^{u_0,u_1,u_3} = -\varepsilon_{K+p}^{-u_0,u_1,-u_3}.$$

This relation partly simplifies the exploration of the parameter space (u_0, u_1, u_3) and we use it to relate the parametric maps for the minibands properties in the valence and conduction bands in graphene.

Figure 3 illustrates characteristic behaviour of the moiré miniband on the valence band side in BLG/hBN for various choices of perturbation parameters and misalignment angles: (a) overlapping minibands characteristic for the transparent part of the parameter space in Fig. 1; (b) gapped spectrum at the edge of the first moiré miniband characteristic for the red-painted part of the parameter space; (c) rare occurrence of a sDP, at the boundary between the above two characteristic regimes. This behavior is shown for both perfectly aligned graphene and hBN lattices ($\theta = 0$) in

Fig. 3(a-c), and for $\theta = 0.597^\circ$ in Fig. 3(d,e). Increasing the misalignment angle leads both to a shorter period of the moiré pattern (reflected by smaller size of dimensionless parameters u_i) and to a rotation of the sBZ, to $\phi = -30^\circ$ for $\theta = 0.597^\circ$ and $\phi = -60^\circ$ for $\theta = 1.836^\circ$ ($vb = 1.89\gamma_1$). We find that this rotation of the moiré pattern interplays with the anisotropy of the warping term $v_3 \sigma \cdot p$ in Eq. (**??**), additionally affecting the occurrence of gapful and gapless miniband spectra. Note that for all angles, there is a gap at zero energy,

$$\Delta \approx 6vbu_0(u_0^2 + u_3^2), \tag{3}$$

between the conduction and valence bands. Opening the gap at the neutrality point of BLG, in the third order of perturbation theory, is analogous to opening a small gap by the inversion symmetry breaking part of the moire perturbation in monolayer graphene, but with the difference that the moiré pattern itself does not have to be inversion asymmetric: the inversion symmetry is broken by the application of substrate perturbation to only one layer out of two. For BLG sandwiched between two hBN layers, the asymmetry will be still present, if the misalignment angles are different, and both the gap Δ and the low-energy dispersion will be determined by that hBN layer which has a smaller misalignment angle. This is because, for the same crystalline substrate, the size of parameters u_i is smaller for larger vb, and the result of Eq. (**??**) suggests scaling $\Delta \propto \theta^{-2}$.

A clear separation between minibands in the spectrum of a periodically modulated two-dimensional semiconductor results in a change of sign of the Hall coefficient as a function of doping[3,9] as the band filling passes the critical values of four electrons per moiré supercell and the chemical potential jumps from the lower miniband to higher (here we take into account spin/valley degeneracy). Such a behaviour has been observed in magneto-transport measurements by Dean et al.,[9] in a similar fashion to monolayer graphene/hBN heterostructures.[3] Since this happens at a relatively high carrier density,[3,9] for which the required large gate voltage introduces an additional interlayer asymmetry, a gap Δ between the conduction and valence band is further enhanced, which can affect spectroscopic characteristics of the system. This purely electrostatic effect.[11,16] is specific to devices with a single-side gate, whereas the spectrum in devices with compensating top and bottom gates would not be affected by doping. To take into account this gate-induced interlayer asymmetry, we add an additional term to Eq. (**??**),

$$\delta\hat{H}_{\Delta} = \frac{1}{2}\Delta \begin{pmatrix} -\sigma_z\tau_z & 0 \\ 0 & \sigma_z\tau_z \end{pmatrix}. \tag{4}$$

and estimate Δ for the carrier density of four electrons per moiré supercell using the mean field theory,[16,17] and find that its presence has almost no effect on the type of the miniband spectrum at the edge of the first miniband (gapped or overlapping minibands), as one can conclude by comparing spectra in Fig. 4 with those in Fig. 3. Therefore, the conclusion on the occurence of the two types of miniband spectra over various parts of the parameter space (u_0, u_1, u_3) in BLG remains virtually the same as illustrated in Fig. 1. Since the systematic study of the moire miniband spectra in BLG shows that the parameter space is dominated by the occurrence of two types of spectra: with a gap separating first and the next miniband, or, alternatively, strongly overlapping minibands (as in weakly modulated semiconductor structures in GaAs/AlGaAS[18–21]), here, we argue that a change in sign of the Hall coefficient in BLG/hBN should be expected to accompany an activation behaviour of conductivity σ_{xx}. This is in contrast to monolayer graphene, where the hBN substrate induces secondary Dirac points at the first miniband edge and thus leads to a finite value in the conductivity maximum at the carier density corresponding to four holes per moiré supercell (see Ref. (9)). Surprisingly, the latter feature of BLG (activation behavior of conductivity at the superlattice-induced resistivity maximum) has not been clearly identified in the experiment in Ref. (9).

This work has been supported by the ERC Advanced Grant *Graphene and Beyond*, EU STREP *ConceptGraphene*, Royal Society Wolfson Research Merit Award and EPSRC Science and Innovation Award.

References

(1) Xue J.; Sanchez-Yamagishi J.; Bulmash D.; Jacquod P.; Deshpande A.; Watanabe K.; Taniguchi T.;, Jarillo-Herrero P.; LeRoy B. J. *Nat. Mat.* **10**, 282 (2011).

(2) Yankowitz M.; Xue J.; Cormode D.; Sanchez-Yamagishi J. D.; Watanabe K.; Taniguchi T.; Jarillo-Herrero P.; Jacquod P.; LeRoy B. J. *Nat. Phys.* **8**, 382 (2012).

(3) Ponomarenko L. A.; Gorbachev R. V.; Elias D. C.; Yu G. L.; Mayorov A. S.; Wallbank J.; Mucha-Kruczynski M.; Patel A.; Piot B. A.; Potemski M.; Grigorieva I. V.; Novoselov K. S.; Guinea F.; Fal'ko V. I.; Geim A. K. arXiv:1212.5012 (2012).

(4) Hunt B.; Sanchez-Yamagishi J. D.; Young A. F.; Watanabe K.; Taniguchi T.; Moon P.; Koshino M.; Jarillo-Herrero P.; Ashoori R. C. arXiv:1303.6942 (2013).

(5) Sachs B.; Wehling T. O.; Katsnelson M. I.; Lichtenstein A. I. *Phys. Rev. B* **84**, 195414 (2011).

(6) Kindermann M.; Uchoa B.; Miller D. L. *Phys. Rev. B* **86**, 115415 (2012).

(7) Ortix C.; Yang L.; van den Brink J. *Phys. Rev. B* **86**, 081405 (2012).

(8) Wallbank J. R.; Patel A. A.; Mucha-Kruczynski M.; Geim A. K.; Fal'ko V. I. arXiv:1211.4771 (2012).

(9) Dean C. R.; Wang L.; Maher P.; Forsythe C.; Ghahari F.; Gao Y.; Katoch J.; Ishigami M.; Moon P.; Koshino M.; Taniguchi T.; Watanabe K.; Shepard K. L.; Hone J.; Kim P. arXiv:1212.4738 (2012).

(10) Lemonik Y.; Aleiner I. L.; Fal'ko V. I. *Phys. Rev. B* **85**, 245451 (2012).

(11) McCann E.; Fal'ko V. I. *Phys. Rev. Lett.* **96**, 086805 (2006).

(12) Kuzmenko A. B.; Crassee I.; van der Marel D.; Blake P.; Novoselov K. S. *Phys. Rev. B* **80**, 165406 (2009).

(13) Kechedzhi K.; Fal'ko V. I.; McCann E.; Altshuler B. L. *Phys. Rev. Lett.* **98**, 176806 (2007).

(14) Schrieffer J. R.; Wolff P. A. *Phys. Rev.* **149**, 491 (1966).

(15) Aleiner I. L.; Efetov K. B. *Phys. Rev. Lett.* **97**, 236801 (2006).

(16) McCann E. *Phys. Rev. B* **74**, 161403 (2006).

(17) Mucha-Kruczynski M.; McCann E.; Fal'ko V. I. *Sol. St. Commun.* **149**, 1111 (2009).

(18) Albrecht C.; Smet J. H.; Weiss D.; von Klitzing K.; Hennig R.; Langenbuch M.; Suhrke M.; Rossler U.; Umansky V.; Schweizer H. *Phys. Rev. Lett.* **83**, 2234 (1999).

(19) Schlosser T.; Ensslin K.; Kotthaus J. P.; Holland M. *Europhys. Lett.* **33**, 683 (1996).

(20) Albrecht C.; Smet J. H.; von Klitzing K.; Weiss D.; Umansky V.; Schweizer H. *Phys. Rev. Lett.* **86**, 147 (2001).

(21) Geisler M. C.; Smet J. H.; Umansky V.; von Klitzing K.; Naundorf B.; Ketzmerick R.; Schweizer H. *Phys. Rev. Lett.* **92**, 256801 (2004).